Effect of π-electron conjugation length on the solvent-dependent S1 lifetime of peridinin

ARTICLE *in* CHEMICAL PHYSICS LETTERS · SEPTEMBER 2008

Impact Factor: 1.9 · DOI: 10.1016/j.cplett.2008.08.056 · Source: PubMed

6 AUTHORS, INCLUDING:

Nirmalya Chatterjee
Ashoka Trust for Research in Ecology and t…
9 PUBLICATIONS **102** CITATIONS
SEE PROFILE

Dariusz M Niedzwiedzki
Washington University in St. Louis
77 PUBLICATIONS **1,236** CITATIONS
SEE PROFILE

Chemical Physics Letters 463 (2008) 219–224

Contents lists available at ScienceDirect

Chemical Physics Letters

journal homepage: www.elsevier.com/locate/cplett

Effect of π-electron conjugation length on the solvent-dependent S_1 lifetime of peridinin

Nirmalya Chatterjee [a], Dariusz M. Niedzwiedzki [a], Takayuki Kajikawa [b], Shinji Hasegawa [b], Shigeo Katsumura [b], Harry A. Frank [a,*]

[a] Department of Chemistry, University of Connecticut, 55 North Eagleville Road, Storrs, CT 06269-3060, USA
[b] Department of Chemistry, Kwansei Gakuin University, 669-1337 Hyogo, Japan

ARTICLE INFO

Article history:
Received 6 June 2008
In final form 13 August 2008
Available online 15 August 2008

ABSTRACT

Peridinin exhibits an anomalous solvent dependence of its S_1 excited state lifetime attributed to the presence of an intramolecular charge transfer (ICT) state. The nature of this state has yet to be elucidated. Ultrafast time-resolved optical spectroscopy has been performed on a synthetic analog, C_{35}-peridinin, having one less conjugated double bond than peridinin. The data reveal the lifetime decreases from 1.5 ns in *n*-hexane to 9.2 ps in methanol, an order of magnitude larger than peridinin. This is the strongest solvent dependence on the lifetime of an S_1 state of a carotenoid yet reported. The data support the view that the S_1 and ICT states are strongly coupled.

1. Introduction

The lowest-lying excited state, S_1, of carotenoids is a state into which absorption from the ground state, S_0, is forbidden on the basis of symmetry and pseudoparity selection rules [1–5]. Both states are characterized by the irreducible representation, A_g^-, in the idealized C_{2h} point group. The forbiddenness of the $S_0(1^1A_g^-) \rightarrow S_1(2^1A_g^-)$ transition rationalizes the well-documented absence of a solvent effect on the $S_1(2^1A_g^-)$ lifetime for most carotenoids because the vanishingly small dipole moment for the transition remains unaffected by changes in solvent polarity and polarizability [6–9]. However, during the course of an ultrafast time-resolved spectroscopic study of the highly-substituted carotenoid, peridinin (Fig. 1), we discovered that it possesses an atypical and striking solvent effect on the lifetime of its lowest excited singlet state [10]. The S_1 lifetime was found to correlate strongly with solvent polarity, and had a value of ~165 ps in the non-polar solvents, *n*-hexane and CS_2, decreasing by a factor of 14 to ~12 ps in the polar solvents, methanol and acetonitrile. In a subsequent study analyzing a systematic series of carotenoids related to peridinin, we traced the effect to the obligatory presence of a carbonyl group in conjugation with the π-electron system of carbon–carbon double bonds [11]. We postulated that the findings were consistent with the presence of an intramolecular charge transfer (ICT) state uniquely formed in carbonyl-containing carotenoids and stabilized in polar solvents [11]. Whether the ICT state is a separate electronic state from S_1, quantum mechanically mixed with S_1 (denoted S_1/ICT in the literature), or simply a unique S_1 state possessing a strong transition dipole moment has been the subject of extensive experimental and theoretical discussion in the literature [10–19]. Experiments on carbonyl-containing, apo-carotenoids [20–23] have revealed a similar solvent dependence on the S_1 lifetime. For example, 12′-apo-β-caroten-12′-al, which has a total of eight conjugated π-bonds (six in a conjugated polyene chain plus one carbonyl and one β-ionylidine ring) has an S_1 lifetime of 220 ps in the non-polar solvent, *n*-hexane, that decreases by a factor of 28 to 8.0 ps in methanol [20]. Experiments on longer apo-carotenoids revealed a diminishing solvent effect with increasing π-electron chain length [21,22]. These results suggest that the perturbation responsible for the solvent effect becomes more important as the conjugated system of π-electron conjugated bonds is shortened.

In order to test this idea, we synthesized an analog of peridinin having one less conjugated carbon–carbon double bond than peridinin (Fig. 1). Standard peridinin is a so-called 'nor-carotenoid' having a C_{37} carbon skeleton rather than the typical C_{40} system present in most carotenoids [24]. The newly synthesized analog has a C_{35} carbon skeleton (hereafter denoted C_{35}-peridinin), but otherwise is structurally identical to peridinin in that it contains the characteristic lactone ring, allene and other functional groups present in the molecule (Fig. 1). As will be shown below, this structural modification leads to the strongest solvent dependence of the lifetime of the S_1 state of a carotenoid yet reported. The lifetime drops by a factor of 160 from 1.5 ns in *n*-hexane to 9.2 ps in methanol. The data are important for revealing the molecular details responsible for the solvent dependence of the lifetime of the S_1 state of peridinin and other carbonyl-containing carotenoids.

* Corresponding author. Fax: +1 860 486 6558.
E-mail address: harry.frank@uconn.edu (H.A. Frank).

0009-2614/$ - see front matter © 2008 Elsevier B.V. All rights reserved.
doi:10.1016/j.cplett.2008.08.056

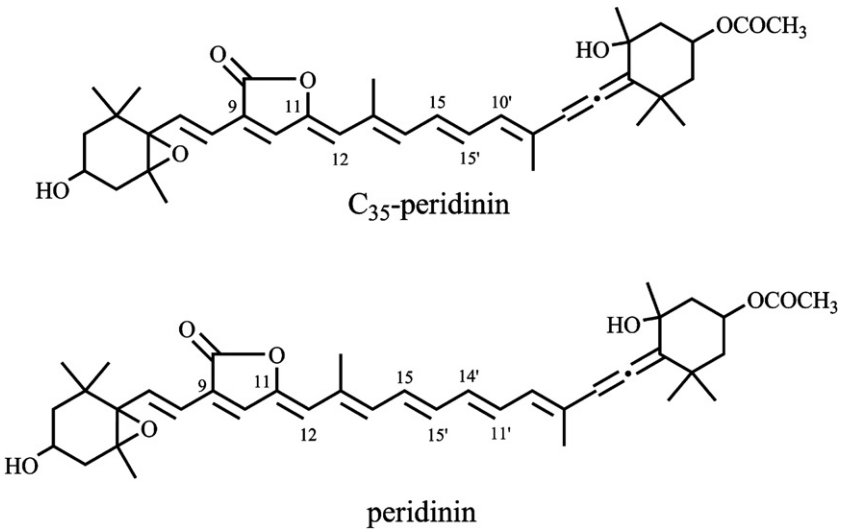

Fig. 1. Molecular structures of C_{35}-peridinin [5,6-epoxy-3′-ethanoyloxy-3,5′-dihydroxy-6′,7′-didehydro-5,6,5′,6′-tetrahydro-11′,12′,13′,14′,20′-pentanor-β,β-caroten-19,11-olide] and peridinin [5,6-epoxy-3′-ethanoyloxy-3,5′-dihydroxy-6′,7′-didehydro-5,6,5′,6′-tetrahydro-12′,13′,20′-trinor-β,β-caroten-19,11-olide].

2. Materials and methods

2.1. Sample preparation

The details of the synthesis of C_{35}-peridinin will be reported elsewhere. C_{35}-peridinin was supplied as a dried sample. Prior to the optical experiments, it was dissolved in acetonitrile and injected into a Millipore Waters 600E high-performance liquid chromatograph (HPLC), using a YMC-Carotenoid C30 column and an isocratic mobile phase protocol. The mobile phase consisted of acetonitrile/methanol (90/10 v/v), and was applied for 15 min at a flow rate of 0.5 mL/min to the column equilibrated under the same conditions for 30 min prior to injection. The sample volume was 200 μL for each injection. The eluent was monitored using a Waters 996 single diode-array detector, and the fraction containing pure C_{35}-peridinin was collected, dried using a gentle stream of gaseous nitrogen and stored at −20 °C until ready for use.

2.2. Spectroscopic methods

2.2.1. Steady-state absorption and fluorescence

C_{35}-peridinin was dissolved in spectroscopic grade solvents obtained from Fisher Scientific (*n*-hexane, 2-propanol) and Aldrich Chemicals (carbon disulfide, ethyl acetate and methanol). Absorption spectra were recorded at 293 K using a Cary 50 UV–visible spectrometer. Fluorescence spectroscopy was carried out using a Jobin-Yvon Horiba Fluorolog-3 model FL3-22 equipped with double monochromators having 1200 grooves/mm gratings, a Hamamatsu R928P photomultiplier tube detector, and a 450 W ozone-free Osram XBO xenon arc lamp. The fluorimeter was set to right-angle detection mode with respect to the excitation beam. The emission spectra were corrected using a file generated from a 200 W quartz tungsten-halogen filament lamp. Both the emission and excitation slit widths were set at 2.5 mm corresponding to a band pass of 5 nm.

2.2.2. Quantum yield measurements

The fluorescence quantum yields of C_{35}-peridinin in the various solvents were determined by integrating the fluorescence profiles shown in Fig. 2 and measuring the results against the integrated emission obtained from a Rhodamine B standard which has a quantum yield of 0.68 in ethanol [25]. The evaluation of the quantum yields was based on Eq. (1) [26]:

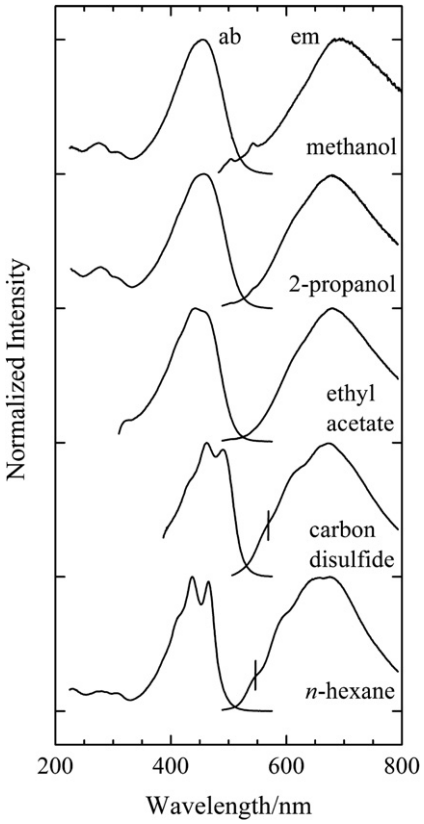

Fig. 2. Steady-state absorption (ab) and fluorescence emission (em) spectra of C_{35}-peridinin taken in various solvents at 293 K. The vertical lines in the emission spectra taken in carbon disulfide and *n*-hexane indicate the $S_1 \rightarrow S_0$ spectral origins based on a Gaussian deconvolution of the vibronic bands in the spectra. The highest energy features correspond to the (0–0) vibronic bands and appear at 565 nm (17 700 cm^{-1}) in carbon disulfide and 545 nm (18 400 cm^{-1}) in *n*-hexane. A slight dip in all the fluorescence spectra due to the Wood's Anomaly appeared at 640 nm and was removed using a correction factor generated from the spectrum of C_{35}-peridinin in methanol.

$$\phi_c = \phi_r \left(\frac{1-10^{-A_{r\lambda}}}{1-10^{-A_{c\lambda}}}\right)\left(\frac{I_{r\lambda}}{I_{c\lambda}}\right)\left(\frac{n_c^2}{n_r^2}\right)\left(\frac{D_c}{D_r}\right) \quad (1)$$

where ϕ_c and ϕ_r are the quantum yields of the C_{35}-peridinin and Rhodamine B solutions, respectively. $I_{c\lambda}$ and $I_{r\lambda}$ are the relative intensities of the excitation light at wavelength λ for the carotenoid and standard solutions. The excitation wavelength was kept constant at 490 nm. $A_{c\lambda}$ and $A_{r\lambda}$ are the absorbances of the carotenoid and Rhodamine B solutions at 490 nm. n_c is the refractive index of the solvents used for the carotenoid (methanol, 1.328; 2-propanol, 1.3776; ethyl acetate, 1.370; carbon disulfide, 1.6276; and *n*-hexane, 1.3749), and n_r is the refractive index of ethanol ($n_r = 1.361$) used for the Rhodamine B standard. D_c and D_r are the integrated areas of the corrected emission spectra of the carotenoid and standard solutions obtained under the identical instrumental conditions of 5 nm band pass.

2.2.3. Transient absorption spectroscopy

Transient absorption spectra were recorded at 293 K on samples adjusted to an optical density between 0.4 and 0.6 in a 2 mm path length quartz cuvette at the excitation wavelength. The femtosecond transient absorption spectrometer system has been previously described [27]. The energy of the pump beam was 1 mJ/pulse in a spot size of 1.2 mm diameter which is equivalent to an intensity of $\sim 1.7 \times 10^{14}$ photons/cm^2 per pulse. The pump wavelength was chosen to be on the long wavelength edge or if evident, into the 0–0 vibronic band of the $S_0 \rightarrow S_2$ of the steady-state absorption spectrum of the molecule. For detection in the visible spectral region, a charge-coupled detector (CCD) with a 2048 pixel array, Model S2000 from Ocean Optics, was used. For detection in the near-infrared region, an SU-LDV Digital Line Scan Camera with a 512 pixel array from Sensors Unlimited was used. Steady-state absorption spectra were recorded before and after all transient experiments to verify sample integrity.

2.3. Results and discussion

Room temperature absorption spectra of C_{35}-peridinin in methanol, 2-propanol, ethyl acetate, carbon disulfide and *n*-hexane, solvents of decreasing polarity, are shown in Fig. 2. The absorption spectrum in the most polar solvent, methanol, is characterized by an intense, broad (FWHM 5330 cm^{-1}) band in the 350–500 nm region. This absorption is associated with the $S_0 \rightarrow S_2$ transition. As the solvent polarity decreases, the absorption band develops resolved vibronic structure as can be seen in the absorption spectrum of C_{35}-peridinin in *n*-hexane (bottom trace in Fig. 2). The longest wavelength feature located at 465 nm corresponds to the spectral origin of the $S_0 \rightarrow S_2$ transition. In the highly polarizable solvent, carbon disulfide, the absorption band is red-shifted due to dispersion interactions, and the spectral origin appears at 490 nm.

Room temperature fluorescence spectra of C_{35}-peridinin are also shown in Fig. 2. In all solvents, the spectra are broad and substantially red-shifted relative to their respective absorption spectra. This indicates that fluorescence emission is occurring from the S_1 state rather than the S_2 state. Also, the fluorescence maxima shift slightly to shorter wavelength and the intensity of emission increases substantially as the solvent polarity decreases. The fluorescence quantum yield was largest in the non-polar solvent, carbon disulfide, and decreased by a factor of ~100 compared to the more polar solvent, methanol (Table 1).

Excitation of C_{35}-peridinin into the S_2 state resulted in a build-up of transient absorption signals shown in Fig. 3. In all solvents except carbon disulfide, spectra taken within 100 fs of the excitation pulse show the build-up of a strong transient absorption signal between 650 and 800 nm. The fact that this signal is completely absent in the spectra taken at longer times, e.g. 1 ps (thick dashed lines in Fig. 3), indicates that it is associated with an $S_2 \rightarrow S_n$ transition whose intensity diminishes rapidly as S_2 is depopulated by internal conversion to form the S_1 state.

The intense transient absorption observed in all the 1 ps traces (dashed lines) in Fig. 3 is due to the characteristic excited state

Table 1
Quantum yields of fluorescence and excited state kinetics of C_{35}-peridinin in different solvents at 293 K

Solvent	ϕ_c	τ
Methanol	$(5.0 \pm 1.2) \times 10^{-4}$	170 ± 10 fs 2.4 ± 0.3 ps 9.2 ± 1.0 ps
2-Propanol	$(2.2 \pm 0.1) \times 10^{-4}$	180 ± 10 fs 6.9 ± 0.5 ps 43 ± 2 ps
Ethyl acetate	$(3.5 \pm 0.4) \times 10^{-3}$	220 ± 10 fs 2.6 ± 0.5 ps 86 ± 5 ps
Carbon disulfide	$(6.4 \pm 0.4) \times 10^{-2}$	410 ± 10 fs 690 ± 60 ps
n-Hexane	$(1.6 \pm 0.1) \times 10^{-3}$	320 ± 10 fs 1.5 ± 0.2 ns

The lifetimes, τ, of the kinetic components were obtained from global fitting the transient absorption datasets. The quantum yields, ϕ_c, were determined as described in the text.

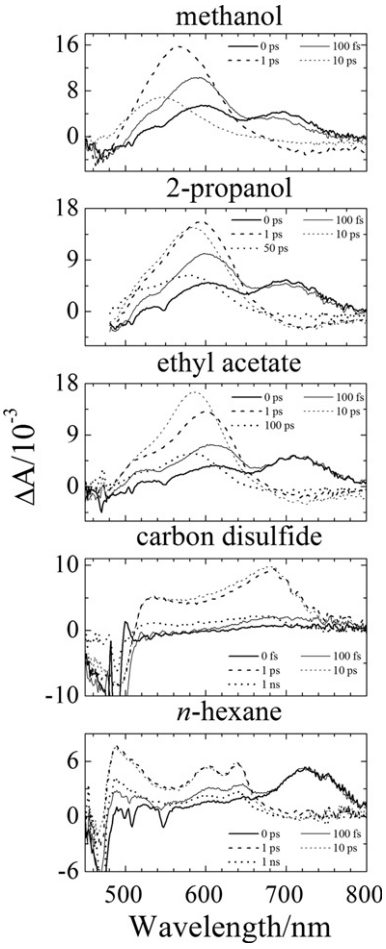

Fig. 3. Transient absorption spectra of C_{35}-peridinin taken at different time delays in various solvents at 293 K.

absorption typically observed for carotenoids. The strong allowedness of this transition gives rise to a substantial solvent effect on the energy of the transition as can be seen from the different positions of the bands in the various solvents. In the polar solvents, methanol, 2-propanol and ethyl acetate, the transient spectra taken at 1 ps are broad and featureless, and as in peridinin and other carbonyl-containing carotenoids, are assigned to an ICT → S_n transition. Moreover, these band maxima shift from longer to shorter wavelength as time elapses. This is very likely due to vibrational cooling in the excited state which has been reported previously for several different carotenoids [28–32]. In the non-polar, highly polarizable solvent, carbon disulfide, the ICT → S_n transition is still observable in the 1 ps trace, but it is shifted out to 680 nm due to dispersion interactions. The $S_1 \rightarrow S_n$ transition in this solvent occurs below 500 nm and is reduced in intensity due overlap with the negative amplitude $S_0 \rightarrow S_2$ absorption bleaching signals. In *n*-hexane two positive bands are seen at 600 and 640 nm in the 1 ps trace in addition to the $S_1 \rightarrow S_n$ transition that appears at 480 nm. The origin of these two positive bands is unclear. They bear a resemblance to the band structure seen between 250 nm and 350 nm in the steady-state absorption spectrum of C_{35}-peridinin in *n*-hexane (Fig. 2). These bands in the UV region of the steady-state spectrum are associated with an $S_0 \rightarrow S_3$ transition and collectively are termed the 'cis-peak' [33]. Summing the energy of the longest wavelength feature appearing at 640 nm (15 600 cm^{-1}) in the transient absorption spectrum of C_{35}-peridinin in *n*-hexane with the energy of the spectral origin of the $S_1 \rightarrow S_0$ fluorescence band appearing at 545 nm (18 400 cm^{-1}, Fig. 2) yields a value of 34 000 cm^{-1} for the energy of the $S_0 \rightarrow S_3$ cis-peak. This corresponds to 294 nm which falls in the UV region where the cis-peak is observed in Fig. 2, suggesting that the two positive bands are due to $S_1 \rightarrow S_3$ excited state absorption. Alternatively, these bands could be due to ICT → S_n transitions that remain evident even in the non-polar solvent, *n*-hexane. In actuality, these two bands may be associated with both $S_1 \rightarrow S_3$ and ICT → S_n transitions. Note that the longer wavelength band at 640 nm is sharper than the shorter wavelength band at 600 nm suggesting different origins. This effect is also observed in the transient absorption spectra of peridinin [9,10].

Fig. 4 shows that the lifetime of the lowest excited singlet state of peridinin is strongly dependent on the solvent. The lifetime is shortest (9.2 ps) in the polar solvent, methanol, and longest (1.5 ns) in the non-polar solvent, *n*-hexane. In order to examine in more detail the nature of this behavior, global fitting of the spectral and temporal datasets were carried out using a model assuming parallel, non-interacting, decay pathways for simultaneously populated excited states [34]. The lineshapes obtained using this model are shown in Fig. 5 and are termed decay-associated difference spectra (DADS). They represent plots of the pre-exponential factors obtained after fitting the datasets to a mathematical sum of exponential kinetic terms. As can be seen in the figure, the first DADS component (light dashed line in Fig. 5) for C_{35}-peridinin in all solvents except carbon disulfide consists of a rapid kinetic component with positive amplitude associated with the $S_2 \rightarrow S_n$ transition above 640 nm that occurs simultaneously with negative amplitude at shorter wavelengths. The positive amplitude represents the decay of the S_2 state and the negative amplitude signals the onset of the vibronically hot $S_1 \rightarrow S_n$ transition. In the polar solvents, methanol, 2-propanol and ethyl acetate, this fast component gives way to an intermediate-time DADS component (thick dashed line) that displays a positive band on the long wavelength side of the major transient absorption signal and a negative band on the short wavelength side. Based on previous studies of peridinin and other carotenoids [32,35], we attribute this behavior to vibronic relaxation in the S_1 state and the transfer of population from the S_1 state to the ICT state [11–13,16–18]. The longest-lived DADS component in all solvents shows features associated with both ICT → S_n and $S_1 \rightarrow S_n$ transitions. Peaks attributable to the $S_1 \rightarrow S_n$ transition are at 480 nm in *n*-hexane, at 520 nm in carbon disulfide, and ap-

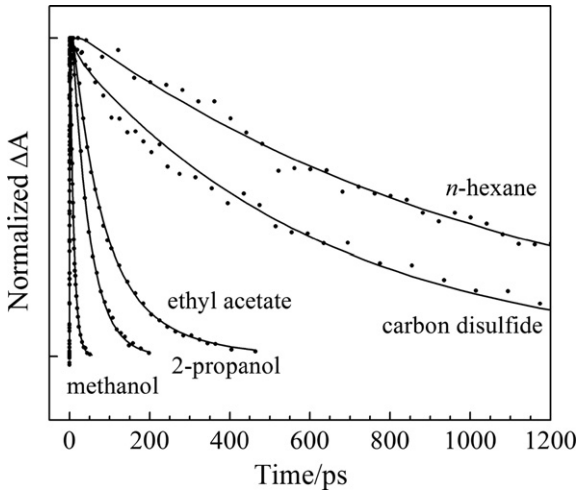

Fig. 4. Normalized kinetic traces of the transient absorption at 293 K. The probe wavelengths were 565 nm (methanol), 580 nm (2-propanol), 585 nm (ethyl acetate), 678 nm (carbon disulfide) and 605 nm (*n*-hexane). The solid lines represent a sum of exponentials fit to the experimental data points.

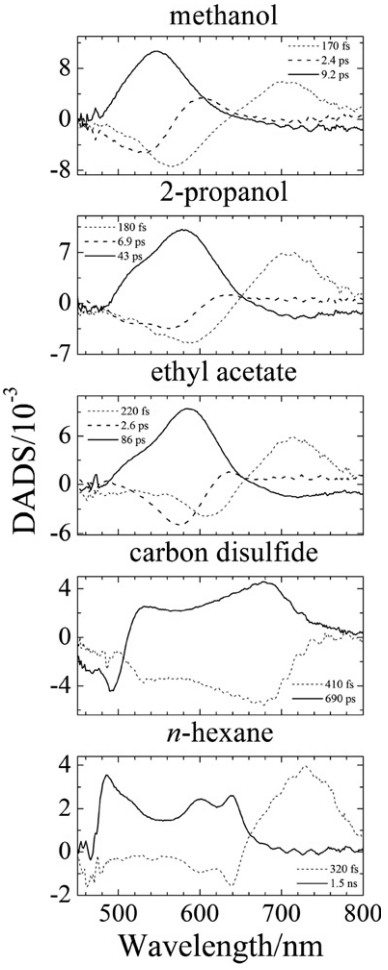

Fig. 5. Decay associated difference spectra (DADS) obtained from global fitting the transient absorption data sets from C_{35}-peridinin.

pear as shoulders at 520 nm for C_{35}-peridinin in ethyl acetate, 2-propanol and methanol (Fig. 5). The observation that features associated with both ICT → S_n and S_1 → S_n transitions appear together in the same, longest-lived DADS component supports the idea that the S_1 and ICT states are strongly quantum mechanically coupled. Spectroscopic features attributable individually to the ICT and S_1 states may appear if the states are associated with different minima on the same (S_1/ICT) potential energy surface [11,13]. If this is the case, alterations in structure or environment that affect one of these states will affect the other as well.

Interestingly, there is an approximate factor of two difference in the lifetime of C_{35}-peridinin in carbon disulfide (690 ps) compared to the value in *n*-hexane (1.5 ns). This may be due to a difference in the S_1–S_0 energy gap in the two solvents brought about by coupling to the ICT state. Typically, the S_1 energy of carotenoids is not sensitive to the solvent environment, but based on the vibronic features resolved in the fluorescence lineshapes of C_{35}-peridinin in these two solvents, (see the vertical lines superimposed on the fluorescence spectra of C_{35}-peridinin in carbon disulfide and *n*-hexane in Fig. 2 indicating the spectral origin of the S_1 → S_0 transition), the S_1 energy of C_{35}-peridinin is higher by ~700 cm^{-1} in *n*-hexane versus carbon disulfide which would lead to a slightly slower S_1 lifetime in *n*-hexane. Note also that the quantum yield of fluorescence of C_{35}-peridinin in carbon disulfide is significantly larger than that observed in *n*-hexane (Table 1). This may be due to a narrowing by ~400 cm^{-1} of the S_2 → S_1 energy gap in carbon disulfide. S_1 fluorescence of polyenes and carotenoids is derived primarily from intensity borrowing via Herzberg-Teller coupling with the S_2 state [36]. Because the energy of the S_2 state of C_{35}-peridinin is significantly lower in the polarizable solvent carbon disulfide compared to *n*-hexane (Fig. 2), the narrower S_2–S_1 energy gap gives rise to a larger fluorescence quantum yield in carbon disulfide.

The data in Fig. 3 for C_{35}-peridinin in the polar solvents, methanol, 2-propanol and ethyl acetate, reveal a negative signal appearing above 650 nm at longer delay times. For peridinin and other carbonyl-containing carotenoids, this signal has been ascribed to stimulated emission from the ICT state. Fig. 6 shows a more complete view of this band extending into the near-infrared spectral region for C_{35}-peridinin in methanol. The absence of the peak in *n*-hexane (Fig. 6) supports the assignment to ICT stimulated emission. The position of the peak at 905 nm to corresponds to an energy of 11 050 cm^{-1} for the ICT state. This compares with the peak position of 930 nm reported for peridinin which corresponds to an ICT state energy of 10 750 cm^{-1} for that molecule [12]. These results indicate that the ICT state of C_{35}-peridinin is only slightly higher than that of peridinin and support our conclusion that in highly polar solvents such as methanol, the energy of the ICT state for both molecules converges to a similar value.

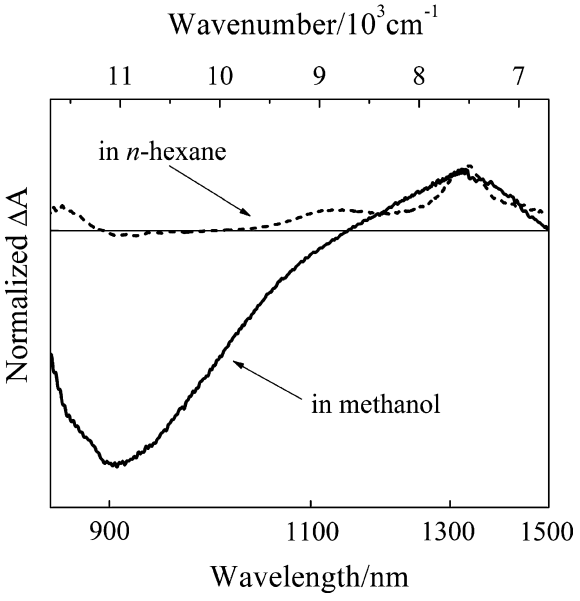

Fig. 6. Transient spectra of C_{35}-peridinin taken in the near-infrared region at 1 ps (in methanol) and 3.5 ps (in *n*-hexane) delay times at 293 K. The spectra were normalized for better visualization.

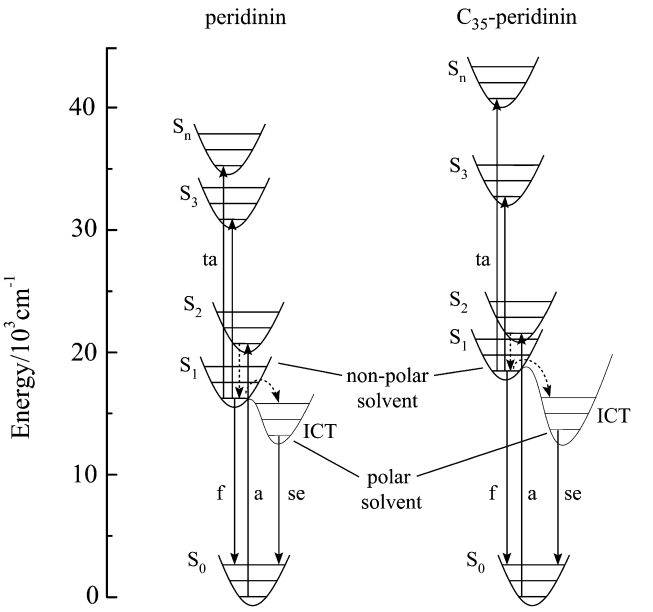

Fig. 7. Potential energy level diagrams and associated spectroscopic transitions comparing peridinin and C_{35}-peridinin in polar and non-polar solvents: ta, transient absorption; f, fluorescence; a, absorption; se, stimulated emission. The solid lines correspond to radiative transitions, and the dashed lines correspond to non-radiative processes.

Fig. 7 shows a potential energy surface diagram depicting the spectroscopic transitions and kinetics of C_{35}-peridinin. The diagram illustrates that shortening the π-electron conjugation of peridinin to form C_{35}-peridinin leads to higher energy excited singlet states which gives rise to a longer S_1 lifetime of C_{35}-peridinin in non-polar solvents. In polar solvents where the formation of the S_1-coupled ICT state is facilitated, the lowest excited singlet state lifetime of C_{35}-peridinin decays with essentially the same time constant as peridinin. This observation, taken together with direct evidence from stimulated emission spectra in the near-infrared region, support the idea that a similar energy gap between the ICT state and S_0 exists for C_{35}-peridinin and peridinin. The representation in Fig. 7 of the S_1 and ICT states as strongly coupled, but having different minima on the same potential energy surface, reconciles the appearance of the distinct spectroscopic observables of fluorescence, transient absorption, and stimulated emission associated with each state, with the simultaneous presence of features associated with both S_1 → S_n and ICT → S_n transitions in the longest-lived DADS kinetic component of the global fit.

Acknowledgements

The authors wish to thank Professors Robert Birge and Tomáš Polívka for useful discussions. This work has been supported in the laboratory of HAF by a grant from the National Institutes of Health (GM-30353) and by the University of Connecticut Research Foundation.

References

[1] R. Pariser, J. Chem. Phys. 24 (1955) 250.
[2] B. Hudson, B. Kohler, Ann. Rev. Phys. Chem. 25 (1974) 437.
[3] P.R. Callis, T.W. Scott, A.C. Albrecht, J. Chem. Phys. 78 (1983) 16.
[4] R.R. Birge, Acc. Chem. Res. 19 (1986) 138.
[5] R.L. Christensen, E.A. Barney, R.D. Broene, M.G.I. Galinato, H.A. Frank, Arch. Biochem. Biophys. 430 (2004) 30.
[6] S. Basu, Adv. Quantum Chem. 1 (1964) 145.
[7] B.S. Hudson, B.E. Kohler, J. Chem. Phys. 59 (1973) 4984.
[8] B.S. Hudson, B.E. Kohler, K. Schulten, in: E.D. Lim (Ed.), Excited States, Academic Press, New York, 1982, p. 1.
[9] T. Polívka, V. Sundström, Chem. Rev. 104 (2004) 2021.
[10] J.A. Bautista et al., J. Phys. Chem. B 103 (1999) 8751.
[11] H.A. Frank et al., J. Phys. Chem. B 104 (2000) 4569.
[12] D. Zigmantas, T. Polivka, R.G. Hiller, A. Yartsev, V. Sundström, J. Phys. Chem. A 105 (2001) 10296.
[13] D. Zigmantas, R.G. Hiller, A. Yartsev, V. Sundström, T. Polivka, J. Phys. Chem. B 107 (2003) 5339.
[14] H.M. Vaswani, C.P. Hsu, M. Head-Gordon, G.R. Fleming, J. Phys. Chem. B 107 (2003) 7940.
[15] S. Shima et al., J. Phys. Chem. A 107 (2003) 8052.
[16] D. Zigmantas, R.G. Hiller, F.P. Sharples, H.A. Frank, V. Sundstrom, T. Polivka, Phys. Chem. Chem. Phys. 6 (2004) 3009.
[17] E. Papagiannakis, D.S. Larsen, I.H.M. van Stokkum, M. Vengris, R.G. Hiller, R. van Grondelle, Biochemistry 43 (2004) 15303.
[18] E. Papagiannakis, M. Vengris, D.S. Larsen, I.H.M. vanStokkum, R.G. Hiller, R. vanGrondelle, J. Phys. Chem. B 110 (2006) 512.
[19] A.J. Van Tassle, M.A. Prantil, R.G. Hiller, G.R. Fleming, Israel J. Chem. 47 (2007) 17.
[20] D.A. Wild, K. Winkler, S. Stalke, K. Oum, T. Lenzer, Phys. Chem. Chem. Phys. 8 (2006) 2499.
[21] F. Ehlers, D.A. Wild, T. Lenzer, K. Oum, J. Phys. Chem. A 111 (2007) 2257.
[22] M. Kopczynski, F. Ehlers, T. Lenzer, K. Oum, J. Phys. Chem. A 111 (2007) 5370.
[23] S. Stalke, D.A. Wild, T. Lenzer, M. Kopczynski, P.W. Lohse, K. Oum, Phys. Chem. Chem. Phys. 10 (2008) 2180.
[24] A. Carotenoids, Birkhäuser, Verlag, Basel, 2004.
[25] F.L. Arbeloa, P.R. Ojeda, I.L. Arbeloa, Chem. Phys. Lett. 148 (1988) 253.
[26] J.N. Demas, G.A. Crosby, J. Phys. Chem. 75 (1971) 991.
[27] R.P. Ilagan, J.F. Koscielecki, R.G. Hiller, F.P. Sharples, G.N. Gibson, R.R. Birge, H.A. Frank, Biochemistry 45 (2006) 14052.
[28] M. Yoshizawa, H. Aoki, H. Hashimoto, Phys. Rev. B 63 (2001) 180301.
[29] F.L. de Weerd, I.H.M. van Stokkum, R. van Grondelle, Chem. Phys. Lett. 354 (2002) 38.
[30] H.H. Billsten, D. Zigmantas, V. Sundström, T. Polívka, Chem. Phys. Lett. 355 (2002) 465.
[31] Z.D. Pendon, G.N. Gibson, I. van der Hoef, J. Lugtenburg, H.A. Frank, J. Phys. Chem. B 109 (2005) 21172.
[32] D. Niedzwiedzki, J.F. Koscielecki, H. Cong, J.O. Sullivan, G.N. Gibson, R.R. Birge, H.A. Frank, J. Phys. Chem. B 111 (2007) 5984.
[33] O. Isler, Carotenoids, Birkhauser, Basel, 1971.
[34] I.H.M. van Stokkum, D.S. Larsen, R. van Grondelle, Biochim. Biophys. Acta 1657 (2004) 82.
[35] D.M. Niedzwiedzki, J.O. Sullivan, T. Polivka, R.R. Birge, H.A. Frank, J. Phys. Chem. B 110 (2006) 22872.
[36] K. Schulten, M. Karplus, Chem. Phys. Lett. 14 (1972) 305.